JOURNAL OF Materials CHEMISTRY

Synthesis, characterization and dehydration study of $H_2A_{0.5n}B_nO_{3n+1}\cdot xH_2O$ ($n=2$ and 3, A = Ca, Sr and B = Nb, Ta) compounds obtained by ion-exchange from the layered $Li_2A_{0.5n}B_nO_{3n+1}$ perovskite materials†

Nattamai S. P. Bhuvanesh,[a] Marie-Pierre Crosnier-Lopez,[b] Huguette Duroy[b] and Jean-Louis Fourquet*[b]

[a]*Department of Chemistry, University of Houston, 4800 Calhoun Blvd., Houston, TX 77204, USA*
[b]*Laboratoire des Fluorures (UPRES A 6010, CNRS), Faculté des Sciences du Mans, Université du Maine, Avenue O. Messiaen, 72085 Le Mans Cedex 9, France. E-mail: jean-louis.fourquet@univ-lemans.fr*

Received 13th January 2000, Accepted 27th March 2000
Published on the Web 30th May 2000

We have synthesized several new layered protonated materials related to Ruddlesden–Popper phases, $H_2A_{0.5n}B_nO_{3n+1}\cdot xH_2O$ (A = Ca, Sr; B = Nb, Ta), by ion-exchange of the lithium ion from $Li_2A_{0.5n}B_nO_{3n+1}$, a family of layered perovskites recently synthesized by us, in dilute HNO_3 at 60 °C. The protonated derivatives show interesting dehydration properties with formation of layered anhydrous phases followed by a transformation to novel metastable $A_{0.5}BO_3$ compounds. The latter oxides, irrespective of the *n*-value of the mother phase, transform on further heating to the thermodynamically stable AB_2O_6 materials. The structural transformations occurring during the dehydration process are characterized by X-ray powder diffraction and electron microscopy techniques.

Introduction

While total syntheses of several organic compounds with complex structures have been achieved by the disconnection approach[1] with the availability of demonstrative examples,[2] rational design in solid state chemistry remains a challenge for well-known reasons.[3] With comprehensive knowledge of structural details, and with an understanding of possible relationships between various known structurally related families, it has been possible to design the synthesis of several solids by a judicial combination of high-temperature ceramic methods and various possible soft-chemical reactions.[4] Examples of such design are shown by the evidence of formation of TiO_2(B),[5] layered brownmillerite,[6] $ACa_2Nb_2AlO_9$, also by suitable substitution, the bridging of the Ruddlesden–Popper (RP) and the Dion–Jacobson (DJ) series in the A–La–Nb–Ti–O system.[7] RP[8] and DJ[9] compounds are two of the well-known series of layered perovskite-related oxides, possessing a general formula $A'_x[A_{n-1}B_nO_{3n+1}]$ ($x=1$ and 2 for DJ and RP phases respectively), where *n* defines the number of BO_6 octahedra forming perovskite layers which are separated by A′ cations. A atoms occupy the 12-coordinated perovskite cages. Various members of these families are known to show a wide variety of chemical and physical properties such as ion-exchange and intercalation,[10] photocatalysis,[11] ferromagnetism and giant magnetoresistance.[12] The difference in the charge of the slabs, which determines the number of interlayer cations (A′), defines the van der Waals attraction between the slabs which in turn decides the mobility of the interlayer cations. Thus, DJ compounds are known to show facile ion-exchange and higher ionic conduction as compared to RP phases.[13]

We have recently reported the syntheses and crystal structures of new oxides of general formula[14,15] $Li_2A_{0.5n}B_nO_{3n+1}$ (A = Ca, Sr; B = Nb, Ta), which belong to a family of oxides related to the layered perovskites of the Ruddlesden–Popper type. Since RP phases are well known to show ion-exchange behavior,[10] we expected the new phases would undergo ion-exchange in aqueous acid. Indeed, we could prepare the compounds $H_2A_{0.5n}B_nO_{3n+1}$ by ion-exchange. Also, based on previous reports of dehydration studies on layered protonated phases,[16–20] we have tried to rationally synthesize novel metastable 3D perovskites with exotic ordering of vacancies: Fig. 1 represents these "hypothetical" compounds for three *n* values (2 to 4). Here, we report the synthesis and characterization of several protonated phases obtained from $Li_2A_{0.5n}B_nO_{3n+1}$ (A = Sr; B = Nb, Ta for $n=2$ and A = Ca, Sr; B = Nb for $n=3$), and the structural changes involved in ion-exchange and further dehydration. The significance of this work is that, in addition to the synthesis

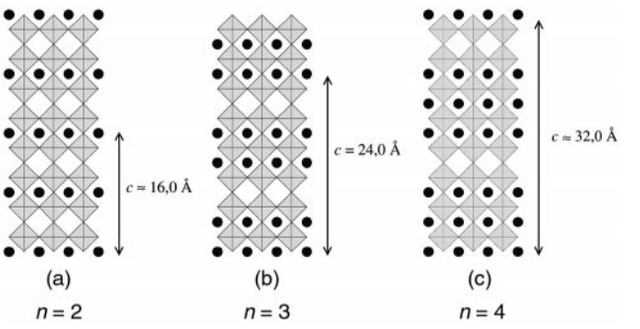

Fig. 1 "Hypothetical" novel metastable 3-D perovskite $A_{0.5}BO_3$ with exotic ordering of vacancies ($n=2$ to 4): small circles represent the A-sites, fully occupied for $n=2$, and with a vacancy rate of 1/4 and 1/3 for $n=3$ and 4, respectively.

†Electronic supplementary information (ESI) available: thermo-XRD patterns, structural characteristics of parent oxides, characteristics of dehydration phases, TG-DTA data for protonated phases. See http://www.rsc.org/suppdata/jm/b0/b000315h/

of novel phases $H_2A_{0.5n}B_nO_{3n+1}$, we have obtained metastable perovskites of composition $A_{0.5}BO_3$, by topotactic dehydration of the protonated phases.

Experimental

$Li_2A_{0.5n}B_nO_{3n+1}$ (A = Ca, Sr; B = Nb, Ta) were synthesized, as reported earlier,[14,15] by reacting stoichiometric quantities of the respective oxides and carbonates. Proton-exchange was carried out by treating 1 g portions of the parent oxides in 100 ml aliquots of 2 M HNO_3 with constant stirring around 60 °C. The solid products were washed and dried in air at room temperature. The Li content analysis of the filtrate using flame photometry indicated that the exchange, in all the cases, was complete after 5 days.

Thermal analysis, thermogravimetric (TG) analysis coupled with differential thermal (DT) analysis, of the proton derivatives was made using a TA instruments SDT 2960 system with a heating rate of 5 to 10 °C min^{-1} under a flowing argon atmosphere. Thermo-X-ray diffractometry was carried out to study the dehydration behavior of the proton-exchanged compounds in air under the following conditions using a Siemens D5000 diffractometer (Cu-Kα radiation): 2θ range 10 to 80°, heating rate 5 °C min^{-1}, delay time 30 min, step scan 0.03°, step time 40 s.

The X-ray powder diffraction (XRD) patterns at room temperature were recorded using a Siemens D-500 diffractometer (Cu-Kα radiation) in the 2θ range 5 to 130° (step scan 0.02°, step time 40 s).

Transmission electron microscopic (TEM) studies, electron diffraction (ED) and high resolution electron imaging (HREM) were carried out using a JEOL 2010 electron microscope operating at 200 kV and equipped with a side entry ±30° double tilt specimen holder. Samples were crushed under n-butanol in an agate mortar. A drop of the suspension was placed on a Cu grid with a holey carbon film and the grid was allowed to dry before examination.

Results and discussion

The structure of $Li_2A_{0.5n}B_nO_{3n+1}$ oxides (Fig. 2) can be described[14,15] as being formed from a perovskite lattice of *n*-BO_6 octahedra (B = Nb, Ta) thick slabs, cut along the *c* direction; these alternate layers are shifted by (*a* + *b*)/2, with the large A cation (A = Ca, Sr) statistically occupying 12-coordinate sites. The lithium ions, found to occupy the interlayer space, are tetrahedrally coordinated. Some of the structural characteristics of the parent oxides used in the present investigation are given as supplementary data in the Electronic Supplementary Information (ESI) (see footnote †). The DT and TG analysis curves for the four protonated phases are shown in Fig. 3, while the thermo-X-ray diffractogram of $H_2Sr_{1.5}Nb_3O_{10}\cdot 0.22H_2O$ is given as Electronic Supplementary Information.† The characteristics of the protonated phases are given as Electronic Supplementary Information.†

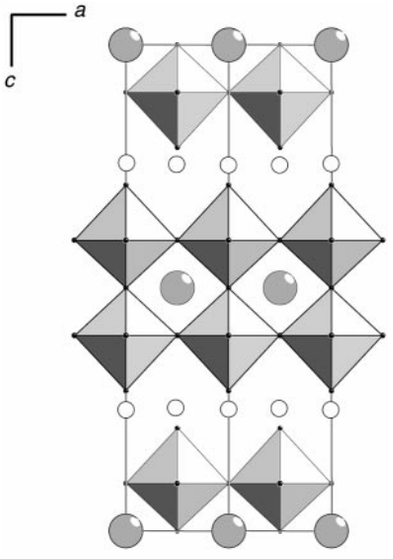

Fig. 2 Structure of $Li_2SrTa_2O_7$ (*n* = 2) showing the perovskite lattice (2-TaO_6 octahedra), the lithium ions (small circles) in the interlayer spacing and the Sr ions (large circles) occupying 12-coordinated sites.

Synthesis and dehydration of $H_2Sr_{1.5}Nb_3O_{10}\cdot 0.22H_2O$

We successfully exchanged all the Li^+ ions in $Li_2Sr_{1.5}Nb_3O_{10}$ topotactically by treating the solid with dilute HNO_3 around 60 °C. While EDX analysis shows that the ratio of Sr to Nb remains the same in the parent and the exchanged phases, the TG analysis (Fig. 3a) of the product shows two weight loss steps (total weight loss = 3.8%). Based on the EDX and TG results we arrived at a formula for the protonated phase of $H_2Sr_{1.5}Nb_3O_{10}\cdot 0.22H_2O$ (calculated weight loss = 3.8%). The X-ray diffraction pattern of the final dehydration product at 800 °C clearly indicates the formation of the $SrNb_2O_6$[21] monoclinic form. The DT analysis curve (Fig. 3a), interestingly, shows three transformations: at 242 °C (sharp endotherm), 470 °C (broad exotherm), and the last one around 680 °C (sharp exotherm). All these transformations are irreversible.

The X-ray diffraction pattern of the exchanged product is closely related to that of the parent phase, as can be seen in Fig. 4, and the presence of strong (00*l*) lines indicates that the layered structure is preserved. Indeed, we could also index the X-ray diffraction pattern of the exchanged product on the basis of a tetragonal cell, as with that of the parent phase.[14] However, we find two significant features in the XRD patterns of the ion-exchanged product: firstly, while the *a* parameter remains the same, there is a considerable expansion of the *c* parameter ($\Delta c \approx 1.67$ Å) associated with the exchange; secondly, a careful examination of the indexing shows that the protonated phase diffractogram can only be indexed on a primitive cell. This kind of structural transformation associated with ion-exchange is well known[17,18,20] in layered perovskites. Sato,[17a] Ollivier[18] and Jacobson[20] and their co-workers have attributed this transformation to a shift of alternate layers: the adjacent layers are stacked immediately above each other in the same arrangement, leading to a *c* axis dimension halved upon proton exchange. In our case, the loss of the *c* axis doubling is not observed, indicating that, if a layer translation occurs during the exchange, two adjacent layers remain translated but with the I-mode violated. On analyzing the systematic absences from the indexation, we find the extinction symbol to be $P4_2--$, with the possible space groups $P4_2$ (No. 77), $P4_2/m$ (No. 84), and $P4_222$ (No. 93). However, we did not succeed in refining the structure, as we found that the full widths at half maximum (FWHM) of the reflections are not uniform: some of the reflections are much broader than the others (see Fig. 4). The presence of broad and sharp lines could be due to a disorder of the water molecules present in the interlayer region, but can also be attributed to some disorder in the layer stacking. It must be pointed out that in the tetragonal cell (proposed space group $P4_2/m$), the pattern matching refinement, carried out by the Rietveld method using the Fullprof program,[22] is not completely satisfactory, since some broad lines are slightly shifted, for example the (102), (106) and (108) reflections. One of the possible reasons for broadening of the reflection peaks may be due to a lower crystal symmetry. Indeed, a best fit is obtained in an orthorhombic cell with $a \approx b$ [$a = 3.9200(4)$ and $b = 3.9337(4)$ Å], but a strong peak overlap makes it difficult to determine the real space group.

Taking into account all these observations, we believe that

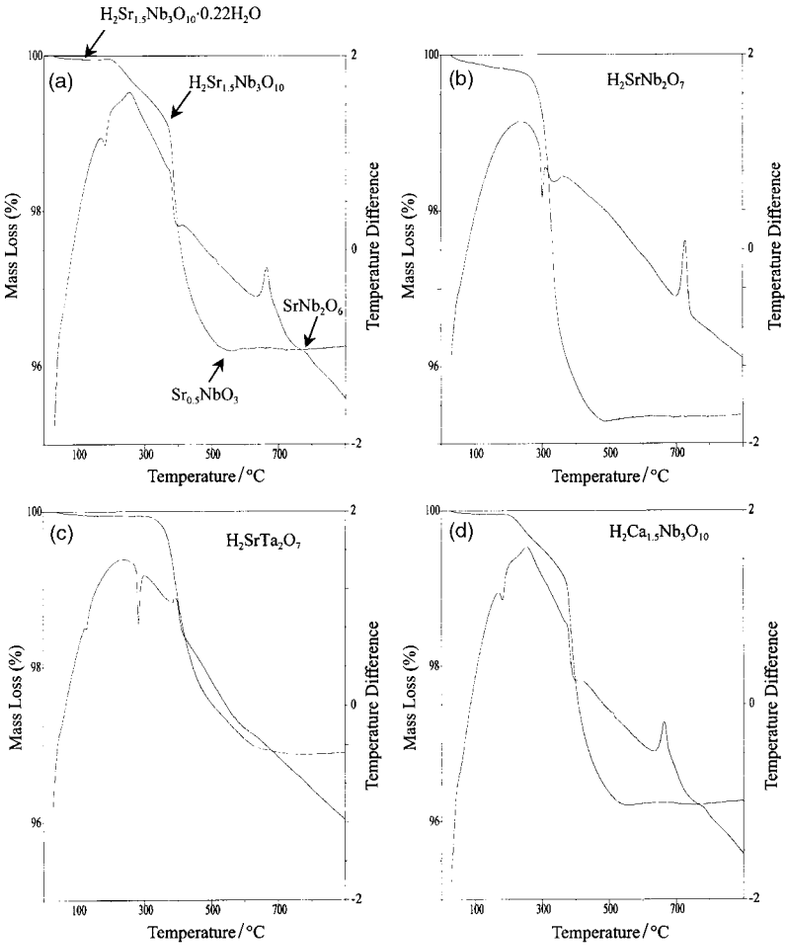

Fig. 3 DT and TG analysis curves for $H_2Sr_{1.5}Nb_3O_{10}\cdot0.22H_2O$ (a), $H_2SrNb_2O_7$ (b), $H_2SrTa_2O_7$ (c) and $H_2Ca_{1.5}Nb_3O_{10}$ (d), showing their dehydration processes.

the structure of $H_2Sr_{1.5}Nb_3O_{10}\cdot0.22H_2O$ is characterized, like the parent phase, by perovskite layers and that two successive slabs remain shifted with the I-mode violated. In such conditions, we can imagine that it is possible to prepare the novel layered $H_2Sr_{1.5}Nb_3O_{10}$ compound on removing the interlayer H_2O, and the three-dimensional $Sr_{0.5}NbO_3$ material on further complete dehydration (Fig. 1b); the structure of the latter oxide could be defined as an ABO_3 perovskite, where A atoms are absent in every third layer along the *c* direction and are present with an occupancy rate of 3/4 in the other layers. This hypothetical process seems in good agreement with the transformations observed in DT analysis: the first two peaks are due to the loss of interlayer water and the loss of protons as H_2O, and the third sharp peak can be attributed to the phase transformation from the metastable $Sr_{0.5}NbO_3$ compound to the thermodynamically stable $SrNb_2O_6$[21] material according to the equations:

$$H_2Sr_{1.5}Nb_3O_{10}\cdot0.22H_2O \rightarrow 0.22H_2O + H_2Sr_{1.5}Nb_3O_{10} \quad (242\,^\circ C)$$

$$H_2Sr_{1.5}Nb_3O_{10} \rightarrow H_2O + 3\,Sr_{0.5}NbO_3 \text{ (Metastable)} \quad (470\,^\circ C)$$

$$2\,Sr_{0.5}NbO_3 \rightarrow SrNb_2O_6\text{[21] (Thermodynamicallystable)} \quad (680\,^\circ C)$$

As there are several changes occurring on heating, as seen in the TG and DT analyses, we carried out a thermo-X-ray diffractometric analysis. The results† clearly show three transformation steps in the X-ray diffraction patterns:

(1) a rapid modification with a decrease in the *c* parameter accompanied by a change from the primitive to body centered cell ($30\,^\circ C < T < 280\,^\circ C$);
(2) a slow change accompanied by a gradual decrease in the *c* parameter, the decrease ceasing around 450 °C;
(3) a rapid change above 600 °C, yielding the thermodynamically stable $SrNb_2O_6$[21] phase.

The X-ray diffraction lines, obtained on dehydration to form $H_2Sr_{1.5}Nb_3O_{10}$ and $Sr_{0.5}NbO_3$, are broad and less intense, whereas the peaks at temperatures above 680 °C, which correspond to the $SrNb_2O_6$[21] pattern, were sharp and intense. Unfortunately, as one can see in Fig. 4, the intensities of the 00*l* lines are strongly affected by the loss of H_2O, and above 400 °C the 002 line disappears completely. However, the lines of the XRD pattern obtained at 530 °C can be indexed only with a tetragonal cell [$a = 3.95(2)$ and $c = 24.1(1)$ Å], the value of the *c* parameter suggesting a three dimensional perovskite ($c \approx 6a_p$, where a_p represents the cell parameter for a regular cubic perovskite). However, the formation of a vacancy-ordered 3D perovskite, which can be easily imagined *via* the loss of protons by removing half the number of the terminal oxygen atoms that point towards the interlayer space in $H_2Sr_{1.5}Nb_3O_{10}$ (see Fig. 1), would imply strong 00*l* lines, as one can see on the simulated (simulation mode of Fullprof) X-ray powder pattern (proposed space group *P*4/*mmm*: one Nb^{5+} at the origin, preserved Nb–O distances and same occupancy rate on the two Sr sites—$a = 3.95$ and $c = 24.1$ Å) shown in Fig. 5. As this simulated pattern is completely different from that observed, we must assume that the water loss implies both a condensation of the layers and a simultaneous migration of the Sr^{2+} cations. Other dehydration mechanisms can be imagined, *e.g.* that proposed by Richard *et al.*[16] for $H_2Nb_2Ti_3O_{10}$. The $Nb_2Ti_3O_9$ phase is obtained at 600 °C by $H_2Nd_2Ti_3O_{10}$ dehydration; the best model proposed by the authors in this case allows a part of the Nd cations to move into the interlayer site: this site is then half occupied by an oxygen and one-third by Nd. When the Nd

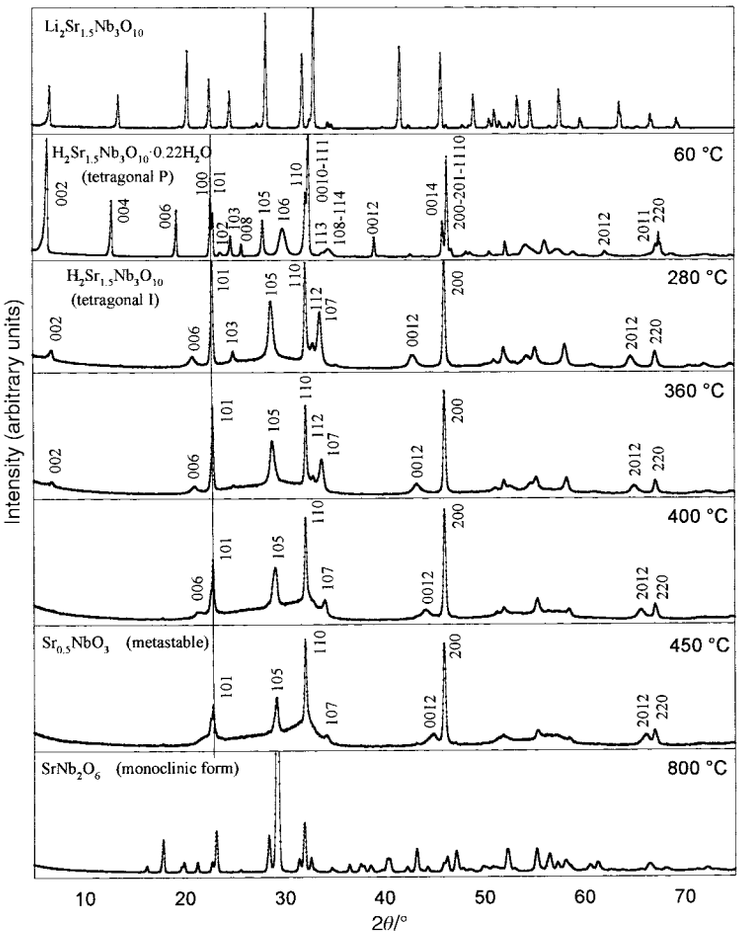

Fig. 4 X-Ray powder diffraction patterns of $Li_2Sr_{1.5}Nb_3O_{10}$ and $H_2Sr_{1.5}Nb_3O_{10}\cdot 0.22H_2O$ at different temperatures showing the vanishing of the 00*l* lines during the dehydration process and the gradual decrease of the *c* parameter.

cation is located on this site, the Ti atom adopts a square pyramidal coordination. However, although this kind of coordination has already been observed in titanosilicates, such a model gives Ti–Nd distances which are too short (close to 2 Å) and thus very improbable.

Although the poor crystallinity of the X-ray diffraction pattern does not allow us to go further in the structure resolution, the $Sr_{0.5}NbO_3$ obtained by us is a novel A-site deficient metastable perovskite. In addition, the latter metastable phase finally yields well crystallized $SrNb_2O_6$ around 680 °C. This clearly provides a low temperature route for the synthesis of pure $SrNb_2O_6$, which is otherwise prepared by heating $SrCO_3$ and Nb_2O_5 above 1200 °C for at least 3 days.[21]

The different steps of this process from the ionic Li^+/H^+ exchange to the dehydration and the transformation into the stable $SrNb_2O_6$ phase are represented schematically in Fig. 6.

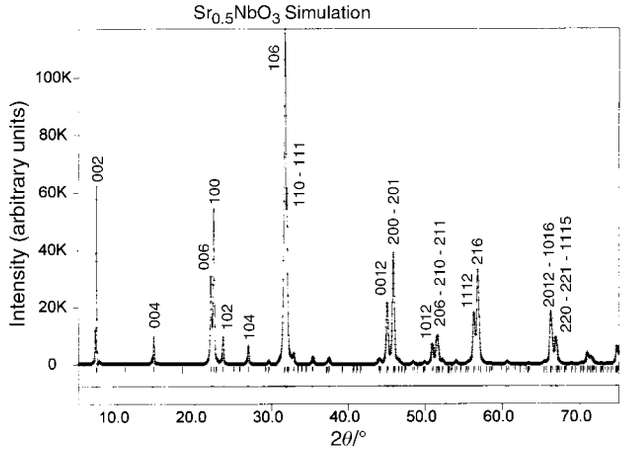

Fig. 5 Simulated X-ray powder diffraction pattern of a "hypothetical" $Sr_{0.5}NbO_3$ vacancy-ordered 3D perovskite obtained from dehydration of $H_2Sr_{1.5}Nb_3O_{10}\cdot 0.22H_2O$ (see Fig. 1).

Ion-exchange and dehydration of other $Li_2A_{0.5n}B_nO_{3n+1}$ phases

$H_2SrNb_2O_7$ ($n=2$), $H_2SrTa_2O_7$ ($n=2$) and $H_2Ca_{1.5}Nb_3O_{10}$ ($n=3$) were also prepared from $Li_2[A_{0.5n}B_nO_{3n+1}]$ materials as described above. The TG analysis reveals that these protonated phases are anhydrous, while the DT analysis shows three transformations for $H_2Sr_2Nb_2O_7$, similar to those occurring in $H_2Sr_{1.5}Nb_3O_{10}\cdot 0.22H_2O$, and four in the case of $H_2SrTa_2O_7$ and $H_2Ca_{1.5}Nb_3O_{10}$.

$H_2SrNb_2O_7$ ($n=2$). As is the case for $Li_2Sr_{1.5}Nb_3O_{10}$, the Li^+/H^+ exchange in $Li_2SrNb_2O_7$ obeys a topotactic mechanism: the XRD pattern of the protonated compound is strongly related to that of the Li^+ phase, with both a substantial increase in the *c* parameter ($\Delta c \approx 1.75$ Å) and a change in the mode (I to P) (Fig. 7a). As mentioned above for $H_2Sr_{1.5}Nb_3O_{10}\cdot 0.22H_2O$, some broad lines are observed and are slightly shifted in a tetragonal symmetry. A protonated phase $HLaNb_2O_7$ has been prepared by Sato and coworkers[17] by K^+/H^+ exchange from $KLaNb_2O_7$, but they have observed that the reaction implied a loss of the *c* doubling due to an $(a+b)/2$ shift of adjacent layers. In our case, if we assume such a shift with the same observed Nb–O distances in the Li^+ phase, it is possible to deduce approximately the distance between the two terminal O atoms of two NbO_6 octahedra facing each other in the interlayer space of the protonated

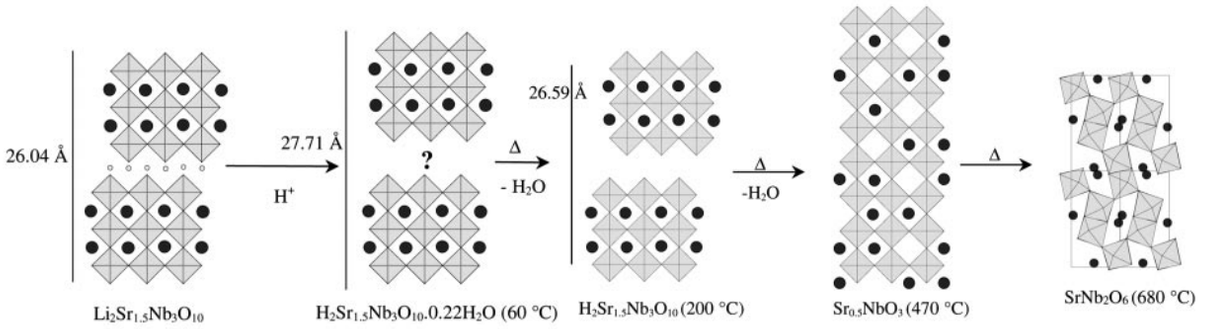

Fig. 6 Schematic structural drawings from $Li_2Sr_{1.5}Nb_3O_{10}$ (RP) to protonated phase $H_2Sr_{1.5}Nb_3O_{10}\cdot 0.22H_2O$ and its dehydration forms, with the formation of the metastable $Sr_{0.5}NbO_3$ (with Sr^{2+} statistically occupying the available 12-coordinate sites) and finally, the transformation to the monoclinic form $SrNb_2O_6$.

phase: the calculated height of the NbO_6 octahedra in the Li^+ phase is 3.86 Å, giving a layer thickness of 7.72 Å, the O–H···O distance can be then estimated as close to 2.16 Å. This distance is really too short compared with those usually encountered in other layered oxides (2.50 Å in $HTiNbO_5$,[23] 2.70 Å in HTi_2NbO_7[23] and 2.85 Å in $HLaNb_2O_7$[17]). Thus, it is clear that in the $H_2SrNb_2O_7$ phase the perovskite layers remain shifted with an I-mode violated.

On heating, the $H_2SrNb_2O_7$ phase shows three transformations, the first two being too close to be separated and occurring simultaneously with the beginning of weight loss. The XRD pattern of the dehydrated phase obtained at 550 °C reveals broad lines which can be indexed in a tetragonal cell: $a\approx 3.94$ and $c\approx 8.60$ Å. This c parameter value is too large compared to that of an expected ordered 3D perovskite (*ca.* 8 Å), resulting from complete condensation. However, this (00*l*) line, which is very broad, attests to great stacking disorder. We can imagine that this $Sr_{0.5}NbO_3$ phase adopts a layered perovskite structure with oxygen vacancies. Such a model, preserving the perovskite layers after complete dehydration, was already proposed for $LaNb_2O_{6.5}$.[17b]

$H_2SrTa_2O_7$. The TG/DT analysis revealed four transformations and a weight loss beginning at higher temperature than those of the other protonated phases (*ca.* 350 °C) (Fig. 3). During its dehydration, several distinct intermediates can be isolated and are shown in Fig. 7b. At room temperature, some of the reflections in $H_2SrTa_2O_7$ are much broader than others and a tetragonal cell similar to that of the parent phase does not allow us to index all the lines. Despite all our efforts, no suitable cell was found with the aid of the Treor program.[24] Thermo-X-ray diffraction revealed that the first two transformations observed at 116 and 280 °C are reversible. The first seems to slightly modify the sliding of the perovskite layers: the XRD pattern of the compound at 200 °C seems very similar to that at room temperature, but the broad lines are a little sharpened and the lines can be indexed in a monoclinic cell [$a=19.353(2)$, $b=3.919(1)$, $c=3.922(1)$ Å and $\beta=96.30(1)°$]. The second exothermic peak is due to a gliding of the perovskite layers, as all the lines of the XRD patterns obtained at 300 °C can be easily indexed in a simple tetragonal cell [$a\approx a_p$ and $c=18.515(2)$ Å] with an extinction symbol $I---$, similarly to the parent phase $Li_2SrTa_2O_7$: two alternate layers are then shifted by $(a+b)/2$. A Rietveld refinement was performed in the *I*4/*mmm* space group using the same structural model as that of $Li_2SrTa_2O_7$ and the *R*-factors converged to acceptable values (Table 1). The calculated O–H···O distance is reasonable: close to 3.12 Å. Taking into account these observations, it is clear that the first two endothermic peaks correspond to a sliding of the perovskite layers.

Ion-exchange on $K_2SrTa_{2-x}Nb_xO_7$ ($x=0.0$, 0.2, 0.4) has been already studied by Ollivier and Mallouk[18] in order to prepare metastable phases $SrTa_{2-x}Nb_xO_6$. They have shown that the X-ray diffraction pattern of $H_2SrTa_{1.6}Nb_{0.4}O_7$ ($x=0.4$) can be indexed in a tetragonal cell with an a parameter close to a_p and a c parameter halved upon proton-exchange [*ca.* 9.87(18) Å]. Classically, they associate this situation with a lateral shift of alternate layers, leading to $(Ta,Nb)O_6$ octahedra facing each other. Taking into account the perovskite layer thickness (*ca.* 7.78 Å), this would imply O–O distances close to 2.09 Å, which seems very unlikely. However, it is interesting to note that the structure of the protonated phase obtained by ion-exchange depends on that of the mother phase, which confirms a topotactic mechanism.

In our $H_2SrTa_2O_7$ compound, between 350 and 600 °C, the loss of H_2O occurs and the metastable phase $Sr_{0.5}TaO_3$ appears. The 00*l* layer lines vanish during dehydration and, at 700 °C, all the sharp lines of the XRD patterns can be indexed in a tetragonal cell with $a=3.93(1)$ and $c=4.00(1)$ Å, while at 600 °C, a broad line (at 2θ close to 8°) implying a doubling of the c parameter is still present. This fact indicates a possible final 3D condensation between 600 and 700 °C, leading to the formation of a disordered perovskite.

Final transformation to the thermodynamically stable $SrTa_2O_6$ compound occurs at much higher temperatures than the other homologues (942 °C) and yields mainly the tetragonal tungsten bronze (TTB) phase $SrTa_2O_6$,[25] with a small amount of an orthorhombic form.[26]

$H_2Ca_{1.5}Nb_3O_{10}$ ($n=3$). The TG analysis shows a two step dehydration process; the observed loss being in good agreement with the formula. As for the mother phase, the X-ray diffraction pattern of the exchanged product (Fig. 7c) can be easily indexed in a tetragonal cell with $a\approx a_p$ and $c=27.340(2)$ Å, leading to a larger c parameter ($\Delta c\approx 1.11$ Å) and an extinction symbol $P4_2--$. However, as discussed previously, a small shift of the broad lines is observed.

Four irreversible transformations are revealed by the DT analysis. At 200 °C, after the first transformation, no weight loss is observed and the lines which violated the I centering mode disappear (Fig. 7c). Indeed, a Rietveld refinement could be easily performed in the *I*4/*mmm* space group by assuming the same structural model as that of the parent phase $Li_2Ca_{1.5}Nb_3O_{10}$ and the *R*-factors converged to acceptable values. The crystallographic data finally obtained are listed in Table 2 and the O–H···O distance calculated (2.96 Å) is reasonable. This first transformation, associated with a change from P to I with a shortening of the c axis (27.34 Å to 26.59 Å) is due to a motion of the layers: at 200 °C, the alternate layers are clearly shifted by $(a+b)/2$. Unfortunately, as for $H_2Sr_{1.5}Nb_3O_{10}\cdot 0.22H_2O$, the exact relative positions of two adjacent layers at 60 °C are not known, despite our efforts to solve the structure.

In 1986, a layered perovskite protonated phase $HCa_2Nb_3O_{10}$ was obtained by Jacobson *et al.*[20] by ion-exchange in aqueous

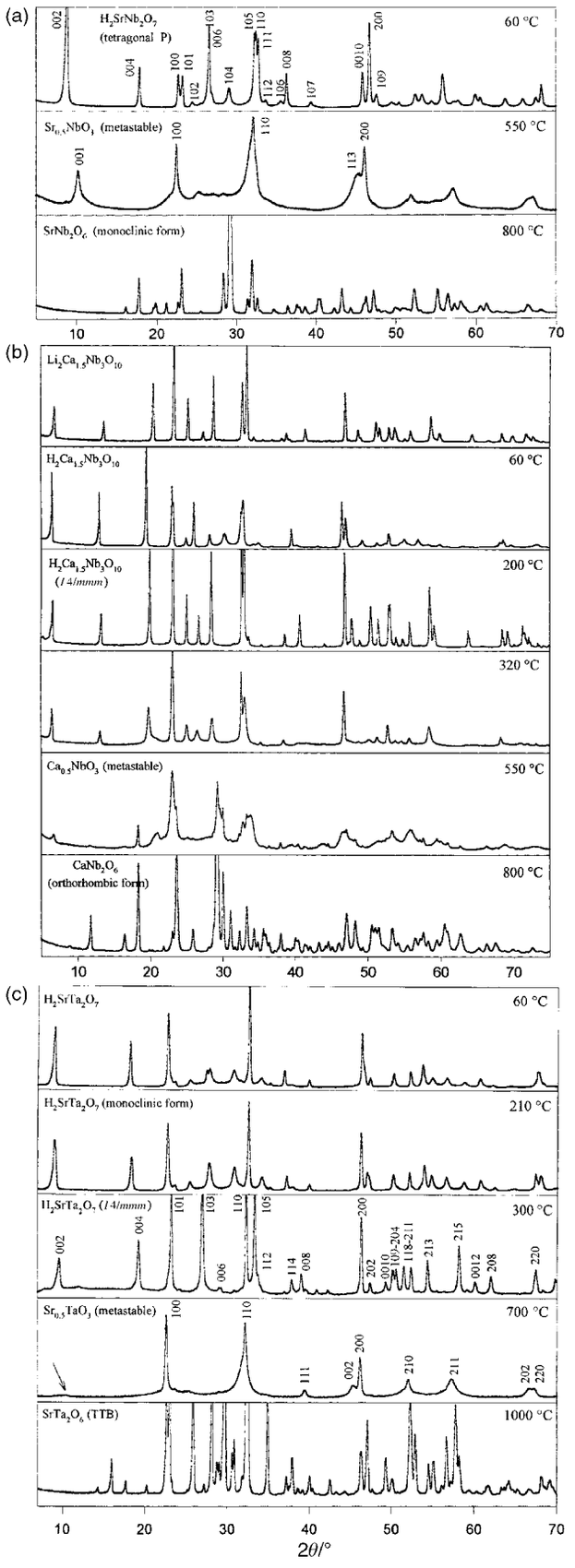

Fig. 7 X-Ray powder diffraction patterns of $H_2SrNb_2O_7$ (a), $H_2SrTa_2O_7$ (b) and $H_2Ca_{1.5}Nb_3O_{10}$ (c) at different temperatures showing the different steps of transformation.

acid from $MCa_2Nb_3O_{10}$ (M = K, Rb, Cs). As for $HLaNb_2O_7$, a topochemical reaction is observed since the layered structure is preserved, but loss of the *c* axis doubling is observed, implying a layer translation. In $HCa_2Nb_3O_{10}$, the O–H···O distance has been estimated to be equal to 2.88 Å, close to values usually encountered. In our case, for $H_2Ca_{1.5}Nb_3O_{10}$, as for $H_2SrNb_2O_7$, such a layer translation would imply too short O–O distances in the interlayer spacing (close to 2.0 Å).

Table 1 Atomic parameters from the Rietveld refinement of $H_2SrTa_2O_7$ at 300 °C[a]

Atom	*x*	*y*	*z*	*B*/Å^2	Site
Ta	0	0	0.3886(1)	0.5(1)	4e
Sr	0	0	0	1.2(1)	2a
O1	0	0.5	0.098(1)	2.6(3)	8g
O2	0	0	0.288(1)	2.6(3)	4e
O3	0	0	0.5	2.6(3)	2b

[a]Note: $a = 3.930(1)$, $c = 18.515(2)$ Å; space group: *I*4/*mmm* (No. 139); $Z = 2$; $R_p = 0.188$, $R_{wp} = 0.180$, $R_{exp} = 0.026$; $R_b = 0.096$. Main distances (Å): Ta–O: 1.852(1), 4 × 1.980(1), 2.063(1) Sr–O: 4 × 2.779(1), 8 × 2.667(1).

For $H_2Ca_{1.5}Nb_3O_{10}$, we observe from the TG analysis that the dehydration started above 200 °C: a strong broadening of some lines and a modification of their relative intensities are then observed in a preserved tetragonal cell. The complete dehydration of $H_2Ca_{1.5}Nb_3O_{10}$ is observed at about 500 °C, and the XRD pattern of the metastable phase $Ca_{0.5}NbO_3$ shows again one small line at a low 2θ value, giving $c \approx 13.3$ Å. However, as in the case of the $H_2Sr_{1.5}Nb_3O_{10}{\cdot}0.22H_2O$ compound, the condensation of the layers to give the expected vacancy-ordered 3D perovskite does not occur. At 590 °C, the orthorhombic phase $CaNb_2O_6$[27] starts to grow with a small amount of a cubic form.[28] Their formation is achieved above 665 °C.

TEM study

In order to confirm the results obtained by X-ray diffraction experiments, we carried out an electron microscopy study: for the protonated phase, only selected area electron diffraction (SAED) was carried out, while for the dehydrated metastable $A_{0.5}BO_3$ compounds, both SAED and high resolution electron microscopy (HREM) was used.

The phases $H_2SrTa_2O_7$ and $H_2SrNb_2O_7$ were investigated by SAED from various crystallites and a scan of the reciprocal space was attempted. However, the crystallites are often very thin platelets with the *c* axis parallel to the electron beam, giving an (001) plane with a first order Laue zone widened, due to the high value of the *c* parameter and the thickness of the sample. A typical SAED pattern observed is shown in Fig. 8a: the spots, intense and sharp, can be indexed in an 'ideal' cubic perovskite cell, without superstructure. In the case of $H_2SrNb_2O_7$, the tetragonal distortion of the orthorhombic symmetry proposed from the X-ray power study seems too small to be revealed by the SAED patterns.

A few crystallites allowed us to get information on the *c* axis, and two examples are given for $H_2SrTa_2O_7$ in Fig. 8b and c, confirming a *c* parameter value close to 19.6 Å. Whereas no defect is evidenced on the [001] zone axis, *c** parallel streaking is observed, indicating disorder along this direction. However, the presence of planar faults or disordered intergrowth gives streaks which pass through every normally allowed reflection. In our case, if the direction of the streaks is always parallel to *c** (classically normal to the slabs which make up the structure), the problem seems more complex, since all the rows are not affected: for example, the 00*l* row presents a perfect *l* even condition, according to the X-ray powder study. Thus, unfortunately, no information about the true cell and the real space group seems to be available.

With regard to the dehydrated metastable $A_{0.5}BO_3$ phases, the compounds $Sr_{0.5}NbO_3$ and $Sr_{0.5}TaO_3$ were studied and were first prepared by heating $H_2SrNb_2O_7$ and $H_2SrTa_2O_7$ respectively at 550 and 600 °C. In the case of $Sr_{0.5}TaO_3$, which

Table 2 Atomic parameters from the Rietveld refinement of $H_2Ca_{1.5}Nb_3O_{10}$ at 200 °C[a]

Atom	*x*	*y*	*z*	*B*/Å^2	Site	Occupancy
Nb1	0	0	0	0.8(1)	2a	1
Nb2	0	0	0.1530(1)	1.0(1)	4e	1
Ca	0.5	0.5	0.0787(4)	2.4(3)	4e	0.75
O1	0	0	0.229(1)	4.0(2)	4e	1
O2	0	0.5	0.147(1)	4.0(2)	8g	1
O3	0	0	0.072(1)	4.0(2)	4e	1
O4	0	0.5	0	4.0(2)	4c	1

[a]Note: $a=3.8711(1)$, $c=26.591(1)$ Å; space group: *I*4/*mmm* (No. 139); $Z=2$; $R_p=0.151$, $R_{wp}=0.171$, $R_{exp}=0.026$; $R_b=0.110$. Main distances (Å): Nb–O: $2\times1.908(1)$, $4\times1.936(1)$, $4\times1.943(1)$, 2.017(1), 2.160(1); Ca–O: $4\times2.648(1)$, $4\times2.744(1)$, $4\times2.851(1)$.

is more stable, the compound was heated for 12 h in order to improve the crystallinity. However, the SAED patterns always show weak and diffuse reflections, as one can see in Fig. 9, revealing a high degree of disorder, in good agreement with the broadening of the lines observed after dehydration in the X-ray powder diffraction pattern. The reconstitution of the reciprocal space leads always to an apparent tetragonal unit cell with a doubling along the *c* axis ($c\approx8.1$ Å). Finally, the corresponding HREM image clearly shows that the phase obtained after dehydration is disordered, as can be seen in Fig. 10. Two extreme situations, A and B, can however be observed in the detail given in Fig. 10: in A, condensation of the layers seems to occur, while in B, the layered structure with a shift of the perovskite slabs is still preserved. However, in A, the doubling along the *c* axis can be only attributed to the formation of the expected metastable and ordered phase $Sr_{0.5}TaO_3$ presented in Fig. 1a.

It is worthy of note that at 600 °C, some crystallites of the phases $SrTa_2O_6$ (TTB form and orthorhombic form) are already formed and very well crystallized, in spite of the high value of the transformation temperature (942 °C).

Conclusion

We have synthesized several new layered protonated phases related to Ruddlesden–Popper phases, $H_2A_{0.5n}B_nO_{3n+1}\cdot xH_2O$ (A = Ca, Sr; B = Nb, Ta), by Li^+/H^+ ion-exchange from $Li_2A_{0.5n}B_nO_{3n+1}$ in dilute HNO_3 at 60 °C. This exchange obeys a topotactic mechanism, since, in all the cases, the layered structure is preserved. All the exchanged products present both

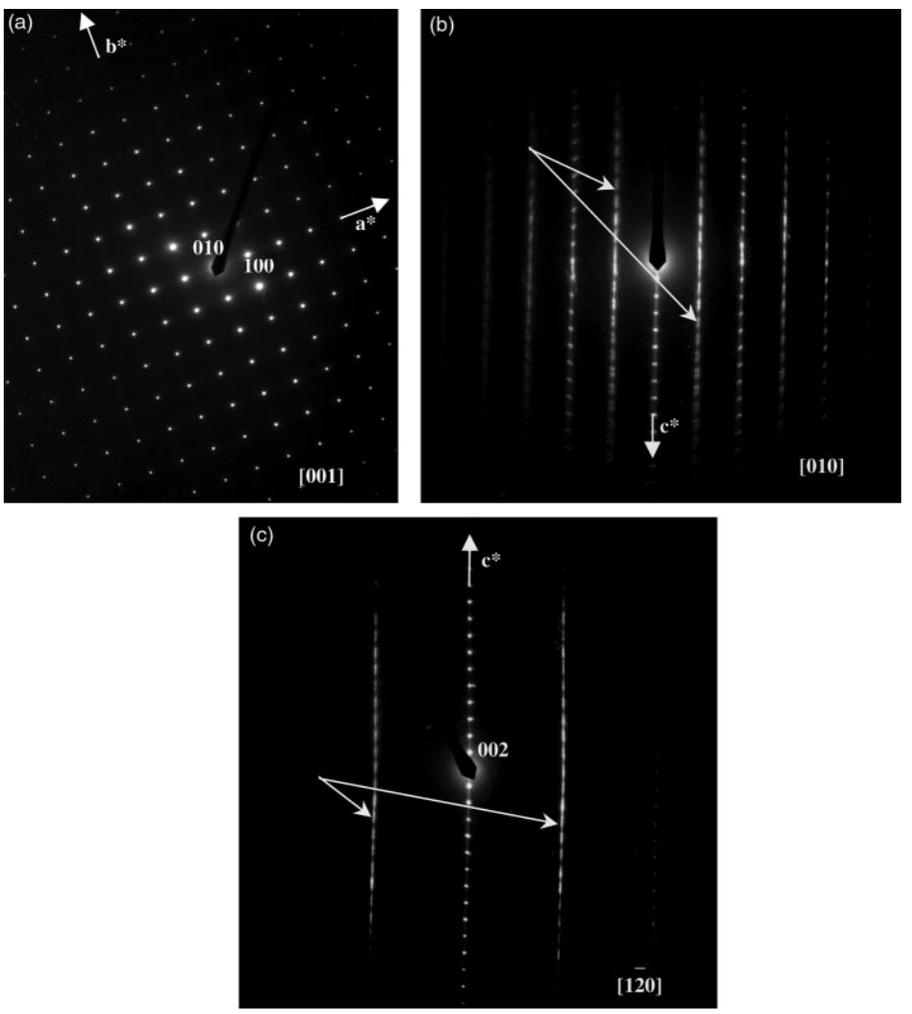

Fig. 8 Typical SAED patterns of $H_2SrTa_2O_7$ showing (a) a perfect [001] zone axis; (b) and (c), streaks parallel to *c** indicating disorder along this direction (Miller indices correspond to spots of a tetragonal cell a_p and $c\approx19.6$ Å).

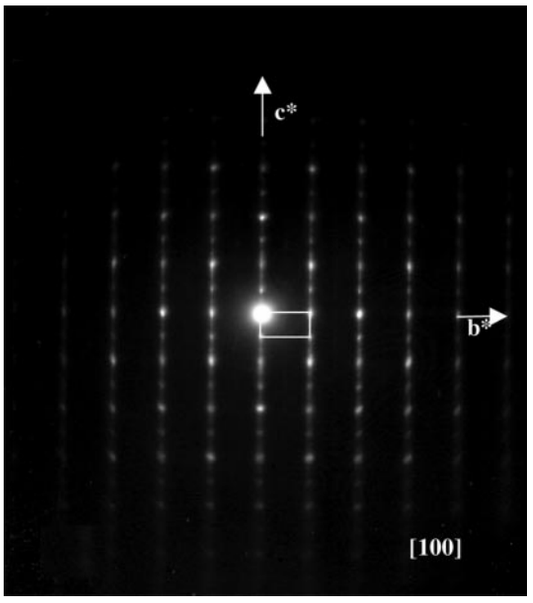

Fig. 9 Typical SAED pattern of $Sr_{0.5}TaO_3$ showing low crystallinity (weak and diffuse reflections), but confirming the doubling along the *c* axis (*ca.* 8.1 Å).

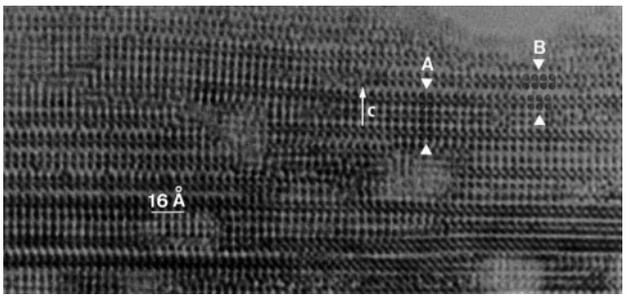

Fig. 10 HREM image of $Sr_{0.5}TaO_3$ showing the coexistence of small domains and giving an SAED pattern such as Fig. 9: in A, condensation of the layers seems to be occurring, while in B, a layered structure with a shift of the perovskite layers is still preserved.

a considerable expansion of the *c* parameter and a change in the mode (I to P) of the unit cell with a broadening of some diffraction lines, indicating some disorder. However, despite our efforts, we have not succeeded in solving the room temperature structures, but, although we do not know the exact relative position of two adjacent layers, the retention of the *c* axis doubling and the calculated O–H···O distances (see text) allow us to imagine that two adjacent layers remain shifted in an I-mode violated fashion. In these protonated phases, the perovskite layers are linked by hydrogen bonding. During the heating, a rapid shrinking of the *c* parameter accompanied by a reverse change from a primitive to a body centered cell is first observed, without weight loss for some protonated phases. Moreover, in the case of $H_2SrTa_2O_7$, the transformation at 280 °C is reversible, showing the "elasticity" of the hydrogen bonding. Then, during the dehydration process, the complete condensation of the layers to give a 3D framework is not always observed. Unfortunately, the expected formation of novel metastable three-dimensional and vacancy-ordered A-site deficient perovskites, $A_{0.5}BO_3$, uniquely determined by the *n* value of the starting proton derivatives, does not seem to occur: on heating, the dehydration process leads to the formation of disordered phases, as revealed by the HREM images obtained for $Sr_{0.5}TaO_3$. However, these $A_{0.5}BO_3$ metastable phases finally transform to the thermodynamically stable AB_2O_6 compounds, irrespective of the *n* value of the mother protonated phase, giving a low temperature route for their synthesis.

Further investigations into the structure determination of the protonated phases are now in progress.

References

1 E. J. Corey and X.-M. Cheng, *The Logic of Chemical Synthesis*, Wiley, New York, 1989; E. J. Corey, *Angew. Chem., Int. Ed. Engl.*, 1991, **30**, 455.
2 N. Anand, J. S. Bindra and S. Ranganathan, *Art in Organic Synthesis*, Holden-Day, San Francisco, 1st edn., 1970.
3 C. N. R. Rao and J. Gopalakrishnan, *New Directions in Solid State Chemistry*, Cambridge University Press, Cambridge, 1986; J. Gopalakrishnan, *Chem. Mater.*, 1995, **7**, 1265.
4 J. Rouxel, M. Tournoux and R. Brec (eds), *Soft Chemistry Routes to New Materials*, Trans Tech Publications Ltd., Switzerland, 1994.
5 R. Marchand, L. Brohan and M. Tournoux, *Mater. Res. Bull.*, 1980, **15**, 1129.
6 S. Uma and J. Gopalakrishnan, *Chem. Mater.*, 1994, **6**, 907.
7 S. Uma, A. R. Raju and J. Gopalakrishnan, *J. Mater. Chem.*, 1993, **3**, 709.
8 S. N. Ruddlesden and P. Popper, *Acta Crystallogr.*, 1957, **10**, 538; S. N. Ruddlesden and P. Popper, *Acta Crystallogr.*, 1958, **11**, 54; A. R. Armstrong and P. A. Anderson, *Inorg. Chem.*, 1994, **33**, 4366; A. J. Wright and C. J. Greaves, *J. Mater. Chem.*, 1996, **6**, 1823.
9 M. Dion, M. Ganne and M. Tournoux, *Mater. Res. Bull.*, 1981, **16**, 1429; M. Dion, M. Ganne and M. Tournoux, *Rev. Chim. Mineral.*, 1986, **23**, 61; A. J. Jacobson, J. W. Johnson and J. T. Lewandowski, *Inorg. Chem.*, 1985, **24**, 3727; J. Gopalakrishnan, V. Bhat and B. Raveau, *Mater. Res. Bull.*, 1987, **22**, 413; M. A. Subramanian, J. Gopalakrishnan and A. W. Sleight, *Mater. Res. Bull.*, 1988, **23**, 837; R. A. Mohan Ram and A. Clearfield, *J. Solid State Chem.*, 1991, **94**, 45.
10 A. J. Jacobson, J. T. Lewandowski and J. W. Johnson, *J. Less-Common Met*, 1984, **21**, 92; A. J. Jacobson, J. W. Johnson and J. T. Lewandowski, *Mater. Res. Bull.*, 1987, **22**, 45; J. Gopalakrishnan and V. Bhat, *Inorg. Chem.*, 1987, **26**, 4299.
11 K. Domen, J. Yoshimura, T. Sekine, A. Tanaka and T. Onishi, *Catal. Lett.*, 1990, **4**, 339; S. Ikeda, A. Tanaka, M. Hara, J. N. Kondo, K. Maruya and K. Domen, *Microporous Mater.*, 1997, **9**, 253; S. Ikeda, M. Hara, J. N. Kondo, K. Domen, H. Takahashi, T. Okubo and M. Kakihana, *Chem. Mater.*, 1998, **10**, 72.
12 Y. Moritomo, A. Asamitsu, H. Kuwahara and Y. Tokura, *Nature*, 1996, **380**, 141; R. Seshadri, C. Martin, M. Herien, B. Raveau and C. N. R. Rao, *Chem. Mater.*, 1997, **9**, 270; P. D. Battle, M. A. Green, N. S. Laskey, J. E. Millburn, L. Murphy, M. J. Rosseinsky, S. P. Sullivan and J. F. Vente, *Chem. Mater.*, 1997, **9**, 552.
13 S. H. Byeon and K. Park, *J. Solid State Chem.*, 1996, **121**, 430.
14 N. S. P. Bhuvanesh, M. P. Crosnier-Lopez, O. Bohnke, J. Emery and J. L. Fourquet, *Chem. Mater.*, 1999, **11**, 634.
15 N. S. P. Bhuvanesh, M. P. Crosnier-Lopez and J. L. Fourquet, *J. Mater. Chem.*, 1999, **9**, 3093.
16 M. Richard, L. Brohan and M. Tournoux, *J. Solid State Chem.*, 1994, **112**, 345.
17 (*a*) M. Sato, J. Abo, T. Jin and M. Ohta, *J. Alloys Compd.*, 1993, **192**, 81; (*b*) M. R. Palacin, M. Lira, J. L. Garcia, M. T. Caldes, N. Casan-Pastor, A. Fuertes and P. Gomez-Romero, *Mater. Res. Bull.*, 1996, **31–32**, 217.
18 P. J. Ollivier and T. E. Mallouk, *Chem. Mater.*, 1998, **10**, 2585.
19 A. J. Jacobson, J. T. Lewandowski and J. W. Johnson, *Mater. Res. Bull.*, 1990, **25**, 679.
20 A. J. Jacobson, J. T. Lewandowski and J. W. Johnson, *J. Less-Common Met.*, 1986, **116**, 137.
21 B. O. Marinder, P. L. Wang and P. E. Wener, *Acta Chem. Scand.*, 1986, **40**, 467.
22 J. Rodriguez-Carvajal, FULLPROF program: Rietveld Pattern Matching Analysis of Powder Patterns, ILL, Grenoble, 1990.
23 B. Raveau, *Rev. Chim. Mineral.*, 1984, **21**, 391.
24 P. E. Werner, L. Erikson and M. Westdhal, *J. Appl. Crystallogr.*, 1985, **18**, 367.
25 B. Henssen, S. A. Sunshine, T. Siegrist, A. T. Fiory and J. V. Waszczak, *Chem. Mater.*, 1991, **3**, 528.
26 V. P. Sirotinkin and S. P. Sirotinkin, *Zh. Neorg. Khim.*, 1993, **38**, 1071.
27 W. Wong-Ng, H. McMurdie, B. Paretzkin, C. Hubbard and A. Dragoo, NBS (USA), ICDD Grant-in-aid, 1988.
28 Krylov and Alekseev, *Zh. Obshch. Khim.*, 1955, **25**, 1052.